Acta Pharmaceutica Sinica B 2021;11(2):544–559

Chinese Pharmaceutical Association
Institute of Materia Medica, Chinese Academy of Medical Sciences

Acta Pharmaceutica Sinica B

www.elsevier.com/locate/apsb
www.sciencedirect.com

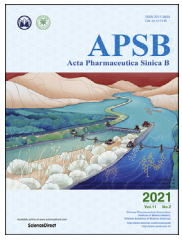

ORIGINAL ARTICLE

# Cathepsin B-responsive and gadolinium-labeled branched glycopolymer-PTX conjugate-derived nanotheranostics for cancer treatment

**Hao Cai[a,†], Yufan Xiang[a,†], Yujun Zeng[a], Zhiqian Li[a], Xiuli Zheng[a], Qiang Luo[a], Hongyan Zhu[b], Qiyong Gong[a], Zhongwei Gu[a], Yanhui Liu[a,*], Hu Zhang[c], Kui Luo[a,*]**

[a]*Huaxi MR Research Center (HMRRC), Department of Neurosurgery, and Department of Radiology, Functional and Molecular Imaging Key Laboratory of Sichuan Province, West China Hospital, Sichuan University, Chengdu 610041, China*
[b]*Laboratory of Stem Cell Biology, West China Hospital, Sichuan University, Chengdu 610041, China*
[c]*Amgen Bioprocessing Centre, Keck Graduate Institute, Claremont, CA 91711, USA*

Received 24 April 2020; received in revised form 8 June 2020; accepted 12 June 2020

**KEY WORDS**

Stimuli-responsive;
Drug delivery;
Branched glycopolymers;
Biodegradability;
Nanomedicine;
Theranostics

**Abstract** Multi-modal therapeutics are emerging for simultaneous diagnosis and treatment of cancer. Polymeric carriers are often employed for loading multiple drugs due to their versatility and controlled release of these drugs in response to a tumor specific microenvironment. A theranostic nanomedicine was designed and prepared by complexing a small gadolinium chelate, conjugating a chemotherapeutic drug PTX through a cathepsin B-responsive linker and covalently bonding a fluorescent probe pheophorbide a (Ppa) with a branched glycopolymer. The branched prodrug-based nanosystem was degradable in the tumor microenvironment with overexpressed cathepsin B, and PTX was simultaneously released to exert its therapeutic effect. The theranostic nanomedicine, branched glycopolymer-PTX-DOTA-Gd, had an extended circulation time, enhanced accumulation in tumors, and excellent biocompatibility with significantly reduced gadolinium ion ($Gd^{3+}$) retention after 96 h post-injection. Enhanced imaging contrast up to 24 h post-injection and excellent antitumor efficacy with a tumor inhibition rate more than 90% were achieved from glycopolymer-PTX-DOTA-Gd without obvious systematic toxicity. This branched polymeric prodrug-based nanomedicine is very promising for safe and effective diagnosis and treatment of cancer.

*Corresponding authors. Tel./fax: +86 28 85422538 (Kui Luo); +86 28 85423622 (Yanhui Liu).
E-mail addresses: liuyh@scu.edu.cn (Yanhui Liu), luokui@scu.edu.cn (Kui Luo).
[†]These authors made equal contributions to this work.
Peer review under responsibility of Chinese Pharmaceutical Association and Institute of Materia Medica, Chinese Academy of Medical Sciences.

https://doi.org/10.1016/j.apsb.2020.07.023

## 1. Introduction

Anti-cancer polymeric conjugates have shown great promise in cancer treatment[1−5]. These conjugates by covalently binding low molecular weight (MW) anticancer drugs to polymers are able to address challenges from current clinical chemotherapeutic medicines, such as nonspecific targeting to tumors and poor solubility in water[6−9]. Polymeric carriers in these conjugates have contributed to enhanced hydrophilicity, increased circulation duration, improved drug stability, and significant permeability and retention (EPR) effect to enter into tumor tissues[10−13]. However, polymers may have inherent toxicity, immunogenicity, undesirable retention and uncontrollable drug release[14−16]. Construction of the conjugation system through tumor microenvironment-responsive linkers, such as disulfide bonds, hydrazone bonds and enzyme-sensitive linkers, has been explored to alleviate the concerns related to the polymers[17−22].

Alternatively, these polymers are modified to reduce inherent toxicity and immunogenicity. For example, polymers with saccharide groups (glycopolymers) have excellent biocompatibility and water-solubility, and these glycopolymers may act as carriers to deliver hydrophobic therapeutic agents[23−25]. Since the glycopolymer with a controllable MW and a low dispersive coefficient can be synthetized *via* reversible addition-fragmentation chain transfer (RAFT) polymerization[26], anti-cancer drugs and imaging probes may be conjugated with the glycopolymer, resulting in a multifunctional glycopolymer-based drug delivery system[27].

In addition, the features of polymers-based drug delivery systems depend on their molecular structures[28]. Among the reported structures, linear and dendritic ones are dominant. Compared with linear ones, branched polymers have a high branched topological structure, a high density of functional groups, a nanoscale size and internal cavities[29]. Especially, functional branched polymers can be prepared *via* one-pot synthesis of RAFT polymerization, and their structures and functions can be optimized *via* selecting and manipulating cross-linking agents and monomers, so they have great application potential as multifunctional polymer delivery systems[30]. Additionally, depending on the choice of tumor microenvironment-responsive cross-linking agents and functionalized side chain groups, the stimuli-responsive branched polymers-based nanoscale drug delivery systems can be achieved with strong EPR effect for negatively-targeting tumors and good biocompatibility. However, at present, glycopolymer-based carriers for drug/gene delivery are mainly derived from linear polymers[25,31].

Herein, a branched glycopolymer-based drug delivery system was designed to accommodate an anti-tumor therapeutic agent, PTX, and two imaging probes, a fluorescence dye pheophorbide a (Ppa) and an magnetic resonance imaging (MRI) contrast agent Gd-DOTA, and this theranostic nanomedicine was constructed (Scheme 1). A branched glycopolymer was chosen as a carrier because this type of polymer has a higher density of functional groups and a large hydrodynamic size, and this branched topological structure is similar to dendritic polymers. To ensure biodegradability and biosafety of the branched polymer, the glycylphenylalanylleucylglycine (Gly-Phe-Leu-Gly, GFLG) tetrapeptide linker was used for fabricating the branched structure because this linker is degradable in the tumor microenvironment with over-expressed cathepsin B in cancer cells. The resulting theranostic nano-assembly was characterized, and the *in vivo* anticancer mechanism, MRI and therapeutic efficacies were determined in a 4T1 xenograft model. Significant inhibition of tumor progression, prolonged and enhanced MRI contrast intensity as well as excellent biocompatibility of this theranostic nano-assembly pave the way for its use in the clinical treatment of cancer.

## 2. Materials and methods

### 2.1. Materials

Gadolinium chloride hexahydate ($GdCl_3 \cdot 6H_2O$), 2,2′-[azobis(1-methylethylidene)]bis[4,5-dihydro-1*H*-imidazole] dihydrochloride (VA044), dithiothreitol (DTT) and cathepsin B were acquired from Sigma−Aldrich (Saint Louis, MI, USA). GAEMA[32], MA-GFLG-PTX[33], MA-DOTA[34], PETMA[35], MA-GFLG-CTA[36], MA-GFLGK-MA[36] and maleimide functionalized Ppa (Maleimide-Ppa)[37] were prepared similarly to one recent report. Other reagents were bought from Aladdin Reagent Co., Ltd. (Shanghai, China) and used as received.

The structures for the intermediate, final product and each monomer were identified through $^1$H NMR (Bruker AVII-400 spectrometer, Bruker Corporation, Billerica, MA, USA), and electron pray ionization mass spectrometry (ESI MS, Waters Corporation, Milford, MA, USA). Size-exclusion chromatography (SEC) with the GE Healthcare column-equipped ÄKTA/FPLC system (GE Healthcare, Chicago, IL, USA) was utilized to measure average molecular weight and polydispersity index (PDI) of polymers. The mobile phase contained sodium acetate buffer with 30% acetonitrile (pH = 6.5) at 0.4 mL/min flow rate through a prepacked Superose 6 HR10/30 electrochromatography column (GE Healthcare, Chicago, IL, USA). Energy dispersive X-ray spectroscopy (EDX) was used to determine the elements contained in the conjugate. The content of various amino acids (including Gly, Phe, Leu and Lys) in the polymer was determined by amino acid analysis. PTX content of conjugate was determined by HPLC (Agilent 1260, Agilent Technologies Inc., Santa Clara, CA, USA) using water/acetonitrile (1:1, *v*/*v*) at 1.0 mL/min and detected by UV absorbance at 227 nm. The amount of Ppa in the conjugate was measured by a fluorescence spectrophotometer (Hitachi F-7000, Tokyo, Japan) after the Ppa-labelled conjugate was dissolved in DMSO ($\lambda_{ex}$ = 405 nm and $\lambda_{em}$ = 673 nm). The fluorescence of free Ppa and glycopolymer-PTX-DOTA-Ppa in PBS with or without 0.1% sodium dodecyl sulfate (SDS) was measured. The Gd(III) content in final products were determined by inductively coupled plasma mass spectrometry (ICP-MS) measurements. The particle size and Zeta potential of polymers dissolved in water were detected through Zetasizer Nano ZS (Malvern Instruments, Malvern, UK). Particle sizes were also

observed under a transmission electron microscopy (TEM, Tecnai G2 F20 S-TWIN, FEI Corporation, Hillsboro, OR, USA). Fluorescence spectra were measured by a fluorescence spectrophotometer (RF-5301-PC, Shimadzu, Kyoto, Japan).

### 2.2. *Preparation of branched glycopolymer-PTX-DOTA-Gd conjugate*

The preparation procedure of branched Glycopolymer-PTX-DOTA-Gd was shown in Supporting Information Scheme S1. GAEMA (1.34 g, 4.38 mmol), MA-DOTA (803 mg, 1.56 mmol), MA-GFLG-PTX (648 mg, 0.5 mmol), PTEMA (31.8 mg, 0.13 mmol), MA-GFLG-CTA (68.9 mg, 72 μmol) and MA-GFLGK-MA (61.5 mg, 93.8 μmol) were weighed and placed into a vial. The vial was protected in an argon atmosphere. The solvent (water/methanol = 1:3, *v*/*v*, 15 mL) with dissolved VA044 (9.0 mg, 28 μmol) were injected into the vial. After the mixture was bubbled with argon for 50 min, the vial was sealed for polymerization at 46 °C in the dark. After 20 h stirring in an oil bath, the polymerization was quenched by liquid nitrogen. The polymer solution was added dropwise into acetone (300 mL) under vigorous stirring, resulting in pink precipitates. The crude products were further purified *via* SEC fractionation. After dialysis and lyophilization, branched glycopolymer-PTX-DOTA (1.63 g, yield 55%) was obtained.

Under an argon atmosphere, the branched glycopolymer-PTX-DOTA (1.5 g) was dissolved in DMSO (15 mL), and dithiothreitol (DTT, 300 mg) was added to the above solution. The mixture was stirred for 10 h and then dialyzed with di-water. After dialysis and lyophilization, the sulfhydryl groups-functionalized product was obtained. In the presence of argon, the product (1.2 g) was chelated with gadolinium *via* reaction of the product with $GdCl_3 \cdot 6H_2O$ (600 mg) in di-water (25 mL) at pH of 5.2−5.4 as previously reported[38]. After dialysis and lyophilization, the

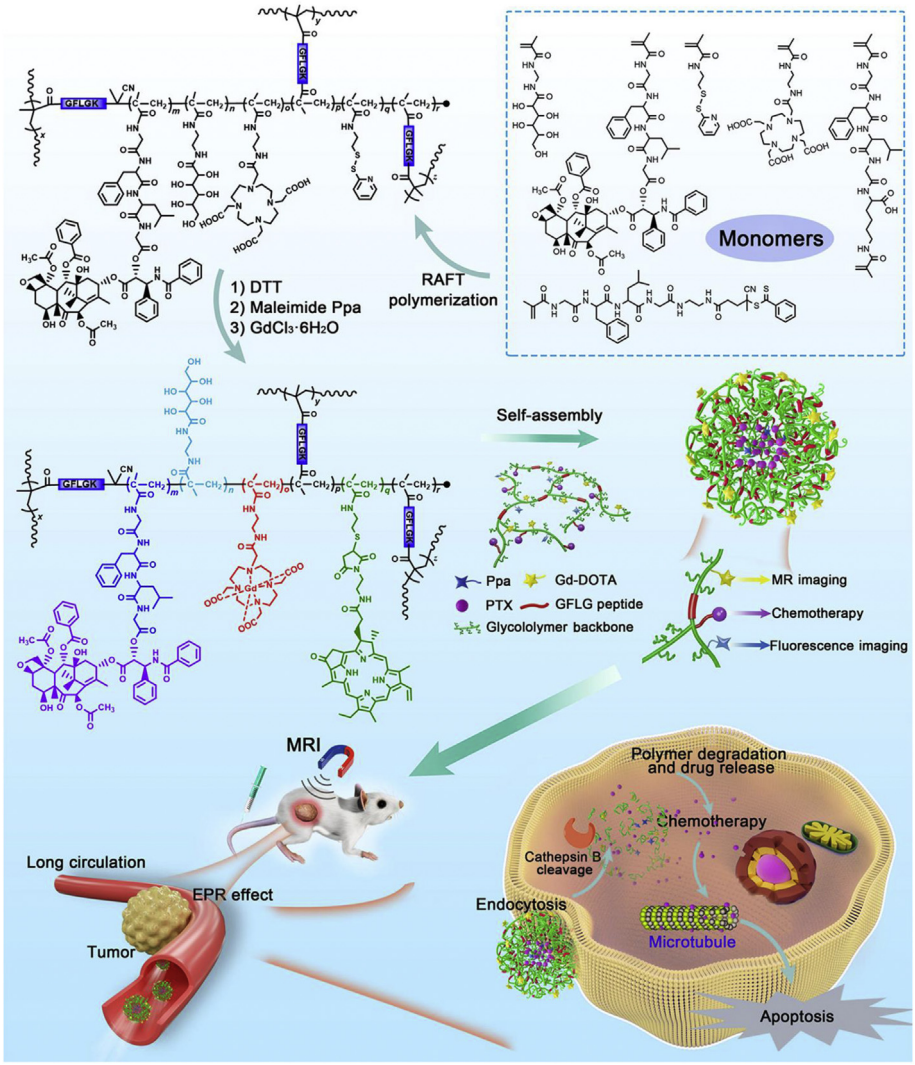


**Scheme 1** Schematic illustration of cathepsin B-responsive biodegradable theranostic nanomedicine based on branched glycopolymer-PTX-DOTA-Gd. Molecular structures of functional monomers and branched glycopolymer-PTX-DOTA-Gd are shown. Branched glycopolymer-PTX-DOTA-Gd is assembled into nanoparticles. The antitumor effect and the MRI enhancement capacity could be boosted *via* the EPR effect to accumulate at tumor sites while circulating *in vivo* for a long duration. Once glycopolymer-PTX-DOTA-Gd is uptaken, the chemotherapy drug PTX is released and the carrier is degraded through interaction with Cathepsin B. The microtubule will be stabilized and apoptosis of tumor cells could be triggered.

gadolinium-labeled polymer was dissolved in DMSO, Maleimide-Ppa (19.7 mg, 30 μmol) in 2 mL DMSO was added to the polymer solution. The mixture was stirred for 6 h. After dialysis against di-water and lyophilization, the final product branched glycopolymer-PTX-DOTA-Gd was obtained. The content of PTX, Ppa and gadolinium in the final product was 6.4%, 0.8% and 4.9% (*w*/*w*), respectively.

### 2.3. Preparation and characterization of branched glycopolymer-PTX-DOTA-Gd nanoparticles

#### 2.3.1. Preparation of nanoparticles

Glycopolymer-PTX-DOTA-Gd nanoparticles were prepared through a dialysis method. Briefly, glycopolymer-PTX-DOTA-Gd (100 mg) was uniformly dispersed into DMSO (10 mL) with a chromatographical purity and the suspension was then slowly added into ultrapure water (10 mL) while vigorous stirring in an ice bath. After 2 h of stirring, DMSO in the solution was removed *via* dialysis at 4 °C. Finally, glycopolymer-PTX-DOTA-Gd nanoparticles were harvested by freeze-drying and then stored at 4 °C for further studies.

#### 2.3.2. Critical association concentration (CAC)

The CAC of glycopolymer-PTX-DOTA-Gd in ultrapure water was determined using a pyrene-based fluorescence probe spectrometry. A series of glycopolymer-PTX-DOTA-Gd solutions at different concentrations (0.25−1000 μg/mL) were accurately prepared. After pyrene ($5 \times 10^{-5}$ mol/L) in 25 μL acetone was dropped into a 10 mL bottle to evaporate acetone, 2 mL glycopolymer-PTX-DOTA-Gd sample solution was added into the bottle to reach a final pyrene concentration of $6.25 \times 10^{-7}$ mol/L. The samples were incubated in a thermostatic oscillator at 37 °C for 2 h and their pyrene fluorescence spectra were recorded through a fluorescence spectrophotometry (emission: 390 nm, excitation: 300−350 nm) and the CAC was determined from the pyrene fluorescence spectra.

#### 2.3.3. Size, zeta potential, morphology and stability

Laser dynamic light scattering (DLS, Zetasizer Nano ZS, Malvern Instruments, Malvern, UK) was used for determination of size and zeta potential of the polymer. Briefly, glycopolymer-PTX-DOTA-Gd was added into deionized water (1 mg/mL) and the solution was applied to a Malvern nanoparticle size and zeta potential analyser (Zetasizer Nano ZS, Malvern Instruments, Malvern, UK). The stability of the nanoparticles in PBS was determined by monitoring any change in the particle size through the same method. Moreover, a TEM (Tecnai G2 F20 S-TWIN, FEI Tecnai Corporation, Hillsboro, OR, USA) was utilized to observe the size and shape of the nanoparticles. The glycopolymer-PTX-DOTA-Gd solution (0.5 mg/mL) was added onto a copper net, dewatered with filter papers, and dried naturally for TEM observation.

### 2.4. Biodegradability and in vitro drug release

Cathepsin B is highly expressed in 4T1 cell line[39,40]. Therefore, we studied the enzyme-responsive degradation and drug release of glycopolymer-PTX-DOTA-Gd by simulating the microenvironment of 4T1 cells. First, biodegradability of glycopolymer-PTX-DOTA-Gd (6 mg/mL) was assessed by adding the nanoparticles into the cathepsin B solution (2.8 μmol/L) with a McIlvaine's buffer (pH = 5.4, 50 mmol/L citrate, 0.1 mol/L phosphate and 2 mmol/L EDTA). The mixture solution was incubated at 37 °C for 0, 2, 6, 12 and 20 h and the molecular weights (MWs) of the polymer was measured through SEC using 1 mL mixing solution. The mobile phase was 70% sodium acetate buffer and 30% methanol (pH 6.5, a flow rate of 0.4 mL/min). Triplicates were prepared for assessment of biodegradability of the polymer.

*In vitro* PTX release from the glycopolymer-PTX-DOTA-Gd (3 mg/mL) nanomedicine was evaluated with a McIlvaine's buffer (pH 5.4, 2.8 μmol/L cathepsin B) after incubation for 24 h at 37 °C, and the final concentration of the polymer was 3 mg/mL. At pre-set intervals, the sample (100 μL) was withdrawn and mixed with 100 μL methanol for HPLC analysis (Zorbax C8 column: 150 mm × 4.6 mm, detection wavelength: 227 nm) with a mobile phase of acetonitrile and water at the equal volume at a flow rate of 1.0 mL/min.

### 2.5. In vitro relaxivity of glycopolymer-PTX-DOTA-Gd and Gd-DTPA

The $T_1$ relaxivity of glycopolymer-PTX-DOTA-Gd was measured on a 1.5 T MRI scanner for glycopolymer-PTX-DOTA-Gd in PBS (0.1 mol/L) with different $Gd^{3+}$ concentrations varying from 0.05 to 0.40 mmol/L. A series of Gd-DTPA solutions with the equivalent $Gd^{3+}$ concentration were also measured. The specific test parameters were described in a previous report[34]. The $r_1$ value was calculated from the following Eq. (1):

$$r_1 = (\text{Slope of } 1/\text{Relaxation time})/Gd^{3+} \quad (1)$$

### 2.6. Cell culture and animals

The 4T1 cell used in this study originated from spontaneous mammary BALB/c carcinoma was acquired from Chinese Academy of Science Cell Bank for Type Culture Collection (Shanghai, China). The cell culture medium, RPMI 1640 (10% fetal bovine serum, 1% penicillin/streptomycin, Life Technologies Co., Carlsbad, USA), was used for culture of the 4T1 cell line in a humidified incubator with 5% $CO_2$ at 37 °C. All mice used in this research were female with BALB/c, weighing 20 ± 2 g and aging from 6 to 8 weeks from DaShuo Biological Technology (Chengdu, China). All animal experimental procedures were conducted by following national regulations and approved by the Animal Ethical Committee of West China Hospital, Sichuan University, China.

### 2.7. In vitro cell uptake and cytotoxicity

The 4T1 cell line was inoculated on a glass dish (35 mm × 12 mm) with 4T1 cells ($1 \times 10^5$ cells/mL) for 24 h. After removal of the spent medium, RPMI 1640 fresh one containing glycopolymer-PTX-DOTA-Gd at an equivalent Ppa concentration of 0.25 μg/mL was placed and cells were incubated for 1, 3 or 5 h. After the medium was aspirated, the cells were rinsed thrice with PBS (pH 7.4) and further incubated in Hoechst 33,342 (10 μg/mL) PBS solution for 15 min. Cells were rinsed thrice with PBS after removal of the dye and observed under a confocal laser scanning microscopy (CLSM).

The CCK-8 kit was employed to study the cytotoxicity of glycopolymer-PTX-DOTA-Gd against 4T1 cells in comparison with free PTX. $5 \times 10^3$ 4T1 cells/well were prepared in 96-well plates, and were treated with glycopolymer-PTX-DOTA-Gd and free PTX at different concentrations ranging from 0.039 to 40 μmol/L for 48 h incubation. Glycopolymer-PTX-DOTA-Gd and

free PTX were aspirated and PBS (pH 7.4) was used to rinse cells thrice before cell viability assessment *via* a CCK-8 kit. The procedure was followed according to the kit manual by recording the absorbance of 100 μL medium with CCK-8 (10%, *v*/*v*) after 2 h incubation *via* a microplate reader and cell viabilities were then calculated.

### 2.8. *In vitro anti-tumor mechanism*

#### 2.8.1. *Cell microtubulin detection*

The 4T1 cell line was inoculated on a glass dish (20 mm in diameter) with 4T1 cells (5000 cells/dish) for 24 h. After removal of the spent medium, cells with fresh RPMI 1640 without any treatment were used as a control. RPMI 1640 fresh ones containing free PTX of 0.5 μg/mL and glycopolymer-PTX-DOTA-Gd at an equivalent PTX concentration of 0.5 μg/mL were placed. All 4T1 cells were incubated for 24 h. After the medium was aspirated, cell tubules were assayed *via* a Tubulin-Tracker Red solution (C1050, Beyotime, Chengdu, China) by following the protocol of the manufacturer. After cell microtubules were stained, the cells were rinsed twice with PBS and further incubated in Hoechst 33,342 (10 μg/mL) PBS solution for 10 min. Cells were rinsed twice with PBS after removal of the dye and observed under a CLSM. The data were further processed by NIS-Elements AR software (Nikon Corporation, Tokyo, Japan).

#### 2.8.2. *Cell proliferation cycle detection*

4T1 cells ($2 \times 10^4$/dish) were seeded in a dish with 5 cm diameter and incubated for 48 h. After removal of the spent medium, fresh RPMI 1640 medium was added, and the PTX concentration for glycopolymer-PTX-DOTA-Gd and free PTX was 0.5 μg/mL. Cells with fresh RPMI 1640 medium without glycopolymer-PTX-DOTA-Gd and PTX were used as a control. Cells were incubated for 24 h, trypsinized and centrifuged after removal of glycopolymer-PTX-DOTA-Gd and free PTX. Proliferation cycle was assayed *via* a PI/RNase Staining Solution by following the protocol of the manufacturer. After cells were fixed and stained, cell proliferation cycle was detected by flow cytometry. The data were further processed by ModFit LT 3.1 software (Verity Software House Inc., Topsham, ME, USA).

#### 2.8.3. *Cell apoptosis detection*

4T1 cells were seeded in a 6-well plate as $5 \times 10^4$ cells/well and incubated for 24 h. After removal of spent medium, fresh RPMI 1640 medium was added, and the PTX concentration for glycopolymer-PTX-DOTA-Gd and free PTX were 1.7 and 1.0 μg/mL, respectively. Cells with fresh RPMI 1640 medium without glycopolymer-PTX-DOTA-Gd and PTX were used as a control. Cells were incubated for 24 h, trypsinized and centrifuged after removal of glycopolymer-PTX-DOTA-Gd and free PTX. Apoptosis was assayed *via* an Annexin V-FITC kit by following the procedure recommended by the manufacturer. After cells were fixed, apoptosis was detected by flow cytometry. The data were further processed by WinMDI 2.9 (The Scripps Institute, San Diego, CA, USA).

### 2.9. *Tumor penetration and depression in three-dimensional multicellular tumor spheroids (MTSs)*

4T1 MTSs were prepared to uncover tumor penetration and inhibition *in vitro*. There was 2 mL molten 2% agarose solution added into dishes of a 5 cm diameter. After solidification of the agarose solution, 4 mL 4T1 cell suspension of $5 \times 10^6$ cells/mL per dish with fresh RMPI 1640 medium was added on the top of agarose. MTSs were formed after about 5-day incubation to reach a diameter of about 200 μm.

To analyze penetration of glycopolymer-PTX-DOTA-Gd, MTSs were assayed with Hoechst33342 by following the protocol of the manufacturer. The MTSs were co-incubated with glycopolymer-PTX-DOTA-Gd for 2 and 6 h. Cells were then observed under a CLSM. The data were further processed by Image J software (National Institutes of Health, Bethesda, MD, USA).

MTS inhibition was measured by staining live and dead 4T1 cells. First, fresh RPMI 1640 medium was added after the MTSs diameter reached about 200 μm, and the PTX concentration for glycopolymer-PTX-DOTA-Gd and free PTX was 2 μg/mL. MTSs with fresh RPMI 1640 medium without glycopolymer-PTX-DOTA-Gd and PTX were used as a control. MTSs were incubated for 48 h and transferred to a 1 mL EP tube after removing the spent medium with or without glycopolymer-PTX-DOTA-Gd and free PTX. Fluorescein calcein AM/propidium iodide (CAM/PI) double staining was used to distinguish live (green) and dead (red) 4T1 cells. The MTSs were assayed by following the protocol of the manufacturer. After MTSs were fixed and transferred to a glass dish, live and dead 4T1 cells were observed under a CLSM. The data were further processed by NIS-Elements AR software (Nikon Corporation).

### 2.10. *Pharmacokinetics and biodistribution analysis*

#### 2.10.1. *Pharmacokinetics analysis*

Pharmacokinetics of glycopolymer-PTX-DOTA-Gd was determined through detection of $Gd^{3+}$ in the plasma at different intervals after injection of glycopolymer-PTX-DOTA-Gd and Gd-DTPA in mice. Healthy BALB/c mice (weight: 20 ± 2 g, $n = 5$) were treated with glycopolymer-PTX-DOTA-Gd conjugates and Gd-DTPA at an equivalent concentration of 0.08 mmol $Gd^{3+}$/kg *via* tail veins, respectively. 20 μL blood samples from each mouse were collected through fundus venous plexus at a pre-set time point after injection and then placed into a centrifuge tube. After complete digestion with $H_2O_2$ and $HNO_3$, the samples were analyzed through detection of the $Gd^{3+}$ concentration *via* an inductively coupled plasma mass spectrometry (ICP-MS). Pharmacokinetic indexes were calculated using the PKSolver 2.0 software[41] (China Pharmaceutical University, Nanjing, China).

#### 2.10.2. *Distribution of glycopolymer-PTX-DOTA-Gd in organs/tissues*

Biodistribution of glycopolymer-PTX-DOTA-Gd in organs/tissues was evaluated *via* fluorescence imaging of these organs/tissues after injection of glycopolymer-PTX-DOTA-Gd into mice bearing 4T1 tumor. The mice with a tumor volume of about 150 $mm^3$ were randomly divided into 2 groups. These mice were injected with glycopolymer-PTX-DOTA-Gd and free Ppa at 1.5 mg Ppa/kg for each mouse *via* tail veins. Three mice of each group were continuously taken fluorescence imaging at 1, 6, 12, 24, 48 and 72 h post-injection.

To make a further understanding of the polymer distribution, every 3 mice of each group were dissected in every same time

point post injection. The major organs (heart, liver, spleen, lung and kidney) and tumor were collected and weighed. Semi-quantitative analysis of fluorescence images of these organs/tissues was carried out *via* a Maestro *In-vivo* imaging system. Mice injected with normal saline were used as a control.

Quantitative distribution of glycopolymer-PTX-DOTA-Gd in organs/tissues was also determined by detecting $Gd^{3+}$ at different time points post injection through ICP-MS. Two groups of BALB/c mice bearing 4T1 tumor ($n = 10$) were randomly formed. The mice were injected with glycopolymer-PTX-DOTA-Gd and Gd-DTPA at an equivalent $Gd^{3+}$ (0.08 mmol $Gd^{3+}$/kg mice) through tail veins. After injection for 24 and 96 h, every 5 mice in each group were sacrificed by cervical dislocation and the major organs (heart, liver, spleen, lung and kidney) and tumors were collected, weighed and completely digested in a mixed solution of concentrated $HNO_3$ and HCl (1:3, *v/v*). The organs/tissues were treated by heating at 120 °C for about 2 days to achieve complete digestion. Deionized water was added to dilute the sample for ICP-MS measurement of the $Gd^{3+}$ concentration in each tissue type. The relative amount of $Gd^{3+}$ was calculated from Eq. (2):

$$\text{Relative } Gd^{3+} = Gd^{3+} \text{ in one organ sample/Mass of the organ sample} \quad (2)$$

### 2.11. *In vivo MRI study*

BALB/c mice bearing 4T1 tumor were randomly distributed into two groups ($n = 5$). Pentobarbital sodium salt was used for anesthesia of all mice and then these mice were fixed in a customized mice coil for MRI imaging in a Siemens Sonata Medical System (Siemens AG, Munich, Germany, magnetic field = 3.0 T), and the imaging parameters were set as previously reported[42]. The glycopolymer-PTX-DOTA-Gd conjugate and the clinical agent Gd-DTPA at a concentration of 0.08 mmol $Gd^{3+}$/kg mice were injected into mice *via* the tail veins, respectively. MRI images were acquired at 10, 30 min, 1, 4 and 24 h post-injection. After all data were collected, the relative enhancement in the signal-to-noise ratio (ΔSNR) was calculated *via* the ratio of the signal intensity (SI) of tumor to that of water [ΔSNR = SI (tumor)/SI (water)]. All values were acquired from the regions of interest in tumor or water. Semi-quantitative assessment of signal changes was carried out by plotting temporal changes of ΔSNR values.

### 2.12. *In vivo antitumor efficacy*

*In vivo* anti-tumor efficacy of glycopolymer-PTX-DOTA-Gd was studied *via* subcutaneous 4T1 tumor models. Female BALB/c mice aging from 6 to 8 weeks were inoculated subcutaneously with 4T1 tumor cells ($1.4 \times 10^5$ cells in 70 μL of PBS) at their right hind legs. After the volume of solid tumors reached 60−80 $mm^3$, these mice were equally divided into three groups ($n = 7$): saline as a negative control, PTX as a positive control and glycopolymer-PTX-DOTA-Gd. Saline, PTX and glycopolymer-PTX-DOTA-Gd were injected into mice every 4 days. For each injection, an equal volume of PTX, glycopolymer-PTX-DOTA-Gd and saline was administrated into the mice and the injection repeated 4 times to reach a dose of 10 mg PTX/kg mice. The tumor geometrical dimensions and weights were recorded on the first experiment day and then every 2 days and their volumes were calculated from Eq. (3):

$$\text{Tumor volume} = (\text{Tumor length} \times \text{Tumor width} \times \text{Tumor width})/2 \quad (3)$$

After 3 weeks, all mice were dissected and the major organs and tumors were collected and weighed. The tumor growth inhibition (TGI) was estimated by Eq. (4):

$$\text{TGI}\ (\%) = (1 - \text{The average weight of tumor of treatment group/The average weight of tumors of control group}) \times 100 \quad (4)$$

In addition, harvested organs of mice after treatment with glycopolymer-PTX-DOTA-Gd were analyzed *via* H&E staining, and the tumor tissues *via* immunohistochemical (IHC) staining, as previously reported[43].

### 2.13. *Immunohistochemistry analysis of CD31and TUNEL assay*

The immunohistochemical (IHC) evaluation was performed using the streptavidin-peroxidase methods[36]. First, after deparaffinaged and rehydrated, the paraffin-embedded tumor sections incubated with monoclonal anti-CD31 antibodies (1:200, Beijing Biosynthesis Biotechnology Co., Ltd., Beijing, China) overnight at 4 °C. Then, the biotinylated goat anti-rabbit antibodies were used as secondary antibodies at 1:200 for 20 min at room temperature. Finally, the IHC images were captured by the Motic Images Advanced software (Ted Pella, Inc., Redding, CA, USA), and the positive-stained integrated optical density (IOD) of the CD31 was scaled with each image by Image-Pro Plus 6.0 software (Media Cybernetics, Inc, Rockville, MD, USA). The tumor microvessel density (MVD) was obtained by calculating the ratio of CD31 of each photograph.

*In situ* terminal deoxynucleotidyl transferase-mediated UTP end labeling (TUNEL) assay was performed using an *in situ* cell death detection kit (Roche Molecular Biochemicals, Laval, Canada) according to the manufacturer's instructions. An optical microscopy was used to observe the positive TUNEL staining and the ratio of the apoptotic cell number in tumor cell number of each microscope field was calculated as apoptotic index.

### 2.14. *Statistical analysis*

Student's *t*-test was applied to statistical analysis of experimental data. All data were presented as mean ± standard deviation (SD). Statistical significance was indicated by $P < 0.05$ and more statistical significance by $P < 0.01$.

## 3. Results and discussion

### 3.1. *Preparation and characterizations of prodrug-based nanosystem*

The schematic route for preparation of the branched glycopolymer prodrug-derived theranostic nanomedicine is provided in (Supporting Information Scheme S1). $^1$H NMR, energy dispersive EDX and SEC were employed in our analysis. As shown at Fig. 1A, a proton peak of glycopolymer-PTX-DOTA is observed at 7.0−8.5 ppm by $^1$H NMR, indicating the existence of aromatic nuclei. The aromatic nuclei might be from Phe produced *via* PTX, Ppa or GFLG. On the other hand, there is no peak in the range of 5.0−6.0 ppm, revealing monomers are completely consumed

because characteristic peaks of double bonds in monomers appear at 5.60 ppm (s, $-CH_3-CH(r)-CH_2-\boldsymbol{H}^a$) and 5.20 ppm (s, $-CH_3-CH(r)-CH_2-\boldsymbol{H}^b$). Elements of C, O, S and Gd are identified by EDX (Fig. 1B), confirming successful conjugation of $Gd^{3+}$ into the glycopolymer. Characteristic peaks of glycopolymer-PTX-DOTA-Gd and free Ppa are detected at 673 nm through fluorescence spectra (Fig. 1C), indicating fluorescence characteristics of Ppa remain unchanged even through the covalent coupling process. The weight percent of the amino acids glycine, phenylalanine and leucine is 2.57%, 3.26%, and 2.54%, resulting in a molar ratio about 2:1:1, indicating the existence of GFLG in the conjugate.

SEC confirms a molecular weight of 244 kDa for glycopolymer-PTX-DOTA-Gd and a PDI of 2.48 (Supporting Information Table S1). All these results support successful production of a multifunctional glycopolymer-PTX-DOTA-Gd conjugate. Hydrophobic PTX and Ppa and hydrophilic glycopolymer chains interact and self-assemble into glycopolymer-PTX-DOTA-Gd nanoparticles. The fluorescent dye Ppa allows tracking the transport route of glycopolymer-PTX-DOTA-Gd inside cells and biodistribution of glycopolymer-PTX-DOTA-Gd in organs/tissues, while the contrast agent Gd-DOTA in the polymer provides real-time imaging of tumor tissues and helps monitoring the pharmacokinetic profile of the nanomedicine *in vivo*.

The size and morphology of glycopolymer-PTX-DOTA-Gd were detected *via* DLS and observed under a TEM. In the presence of both hydrophilic glycosyl chains and hydrophobic chemotherapy drugs, glycopolymer-PTX-DOTA-Gd self-

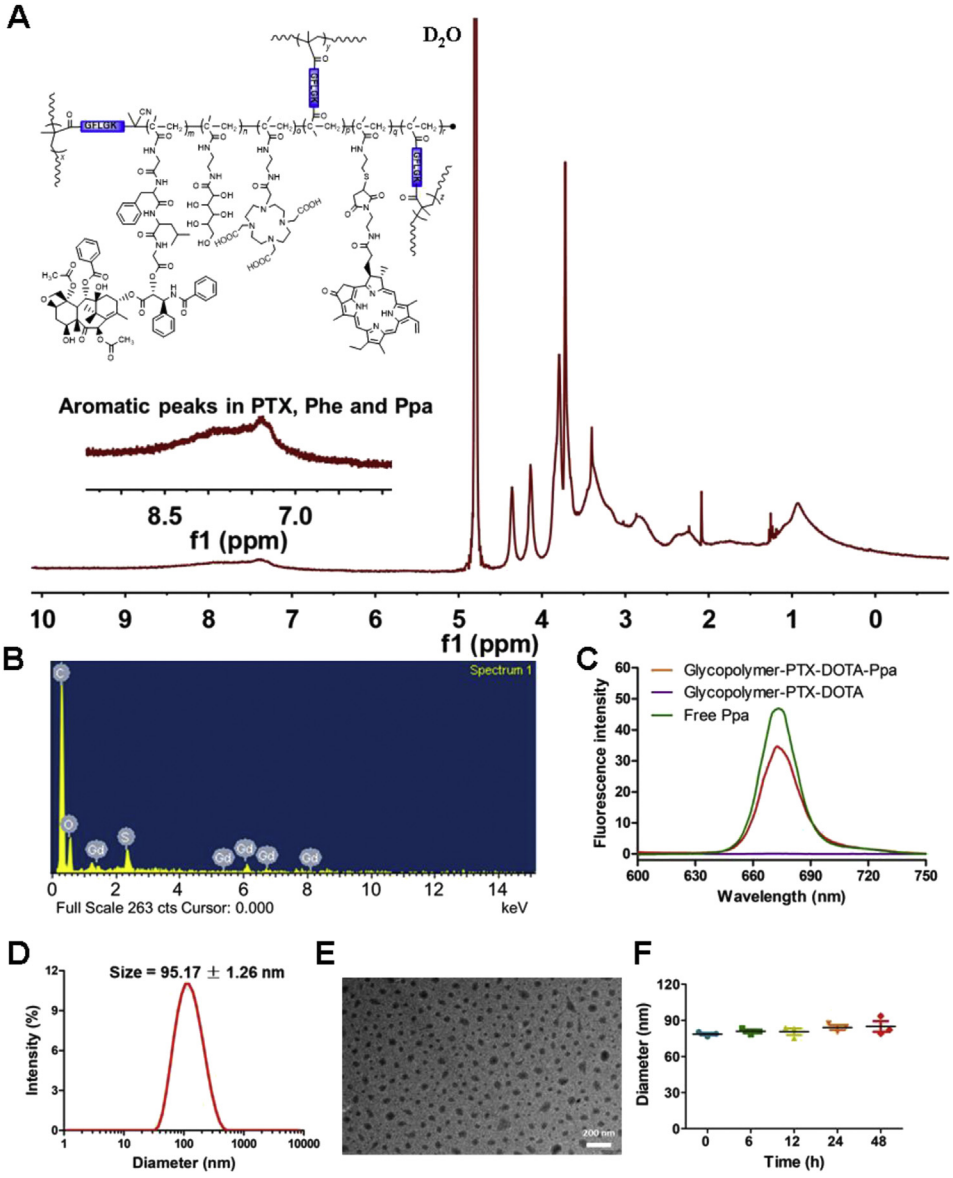


**Figure 1** (A) The $^1$H NMR of branched glycopolymer-PTX-DOTA prodrug. (B) The EDX spectrum of the prodrug. (C) Fluorescence spectrucm of the glycopolymer-PTX-DOTA-Gd prodrug before and after conjugated Ppa, free Ppa was used as control (dissolved in DMSO). (D) Particle size of glycopolymer-PTX-DOTA-Gd in water. (E) Morphology of glycopolymer-PTX-DOTA-Gd *via* TEM. (F) Physical stability of glycopolymer-PTX-DOTA-Gd in PBS.

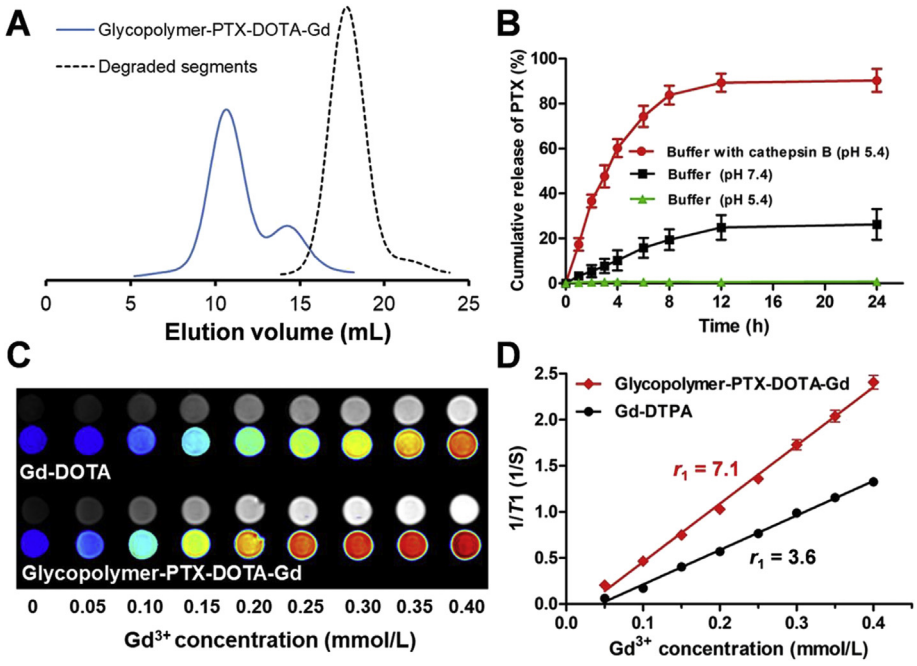


**Figure 2** (A) SEC profiles for glycopolymer-PTX-DOTA-Gd and its biodegraded products after incubation with cathepsin B for 20 h. (B) PTX release curve in three mimicking conditions (mean ± SD, $n = 3$). (C) Contrast images of Gd-DTPA and glycopolymer-PTX-DOTA-Gd at a serial of concentrations and (D) their $T_1$ relaxivity efficacy.

assembles into a theranostic nano-scale structure in water. Fig. 1D shows a hydrodynamic diameter of 95.17 nm for glycopolymer-PTX-DOTA-Gd from DLS. TEM images confirm a uniform size distribution of the conjugate with a spherical shape at around 70 nm in diameter (Fig. 1E). In order to passively accumulate glycopolymer-PTX-DOTA-Gd in the tumor tissue *via* enhanced permeate and retention (EPR) effect, the nanoparticle size is ideally in the range of 10−150 nm and the glycopolymer-PTX-DOTA-Gd nanoparticle size falls within this range[44,45]. Additionally, glycopolymer-PTX-DOTA-Gd conjugate has a zeta potential of 0.336 mV (Supporting Information Fig. S1), which indicates it may extend its blood circulation time to obtain a high level of accumulation at tumor sites since a neutral or negative surface charge of nanoparticles prevents capture of these nanoparticles by serum proteins and macrophages. The CAC of glycopolymer-PTX-DOTA-Gd reaches a low value of 23.7 μg/mL (Supporting Information Fig. S2), which suggests the conjugate at the concentrations used in this study far above the CAC is able to maintain a very stable nano-size assembly structure. The stability of glycopolymer-PTX-DOTA-Gd in PBS is further revealed with negligible changes in particle size after dissolving glycopolymer-PTX-DOTA-Gd in PBS for 48 h (Fig. 1F). Quenching of the fluorescence signal of glycopolymer-PTX-DOTA-Gd in PBS in Supporting Information Fig. S3 also supports successful assembly of the conjugate into a nano-scale structure.

### 3.2. *In vitro degradation, drug release and relaxivity studies*

Previous studies have demonstrated that if a molecular weight (MW) of a polymer is higher than the renal threshold (45 kDa), it is very challenging to eliminate the polymer through normal metabolic pathways in the body[33,46]. Thus, it is vitally important to prepare a nanoscale polymeric drug delivery vector with a MW above the renal threshold that is biodegradable into small fragments for renal clearance. Glycopolymer-PTX-DOTA-Gd was prepared by using MA-decorated GFLG peptide as a cross-linker, which is biodegradable in the micro-environment with highly expressed cathepsin B in tumor cells. To confirm its biodegradation of glycopolymer-PTX-DOTA-Gd, the polymer conjugate was incubated in a mimicking tumor microenvironment: pH = 5.4 and 2.8 μmol/L cathepsin B. As shown in Supporting Information Table S2, the MW of glycopolymer-PTX-DOTA-Gd decreases along with the incubation time up to 20 h. Fig. 2A shows that after incubation with cathepsin B, the peak time of the degraded products of glycopolymer-PTX-DOTA-Gd was significantly extended. It is worth noting that the curve of glycopolymer-PTX-DOTA-Gd has a sharp tail peak, which may be due to a large PDI (2.48) of the polymeric conjugate with a branched structure, and the product may contain a small fraction of polymers with a lower molecular weight. These results confirm the tumor microenvironment-responsive biodegradation of the polymer conjugate. Because of the degraded fragments (28 kDa) with a MW smaller than 45 kDa, bio-degradation endows safe metabolism and rapid elimination of glycopolymer-PTX-DOTA-Gd in the human body. The stable characteristics of the polymeric conjugate in the physiological condition also prolong its circulation time.

Very similar to the biodegradation results, PTX is demonstrated to release in the buffer of pH 5.4 with cathepsin B, and the accumulated release reaches up to 90% for an incubation time of 24 h. However, very little PTX (less than 3%) is released in the buffer of pH 5.4, and a small amount of PTX in the buffer of 7.4 (around 25% for 24 h, Fig. 2B). The result suggests the PTX release is dependent on the concentration of cathepsin B, but not on pH, and disintegration of the polymer conjugate structure leads to release of PTX from the conjugate.

The MRI efficacy of the glycopolymer conjugate was assessed *via* its longitudinal relaxation rate or the relaxivity on a clinical

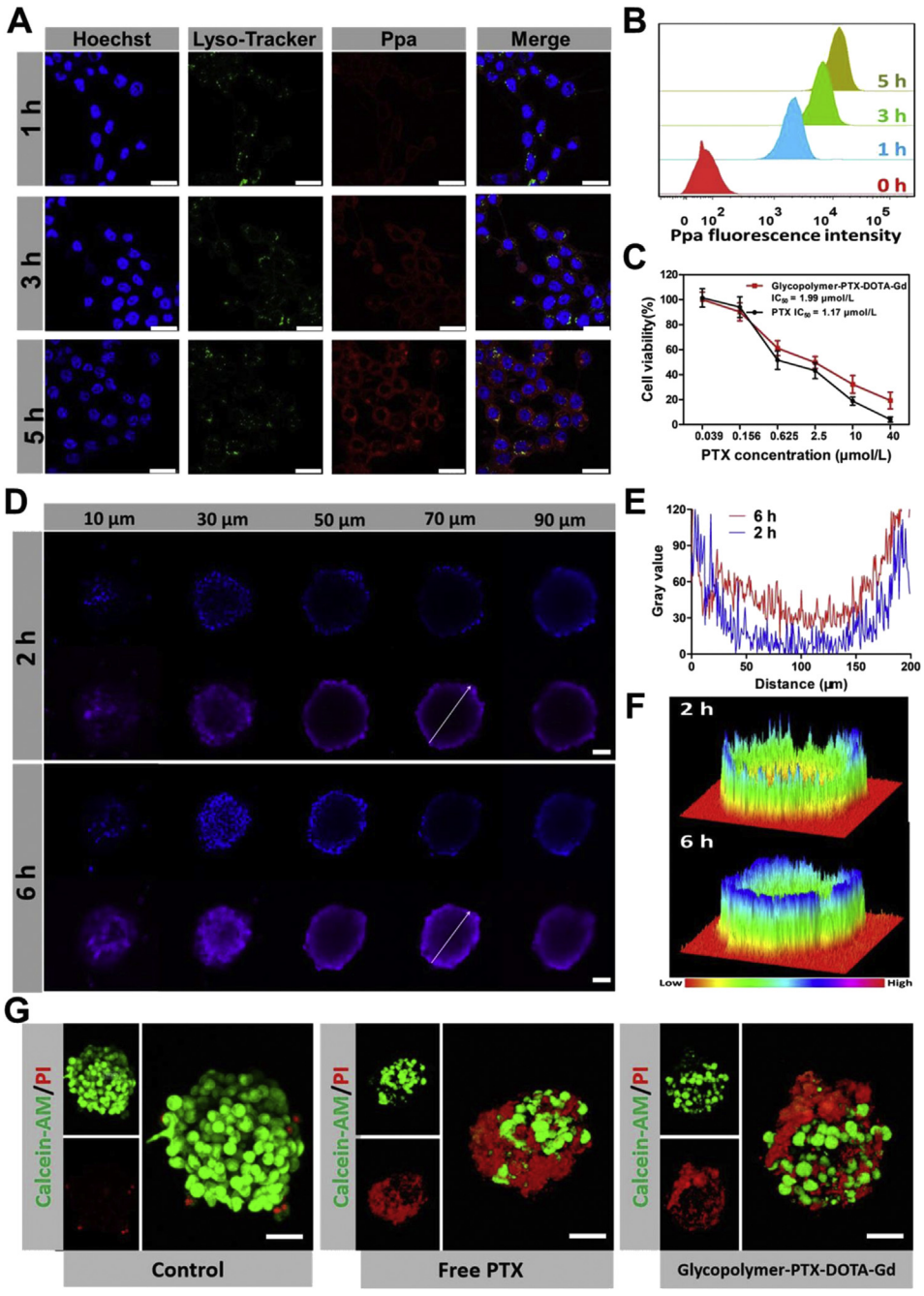


**Figure 3** (A) 4T1 cellular uptake of glycopolymer-PTX-DOTA-Gd at different incubation time observed under a CLSM. (B) Flow cytometric analysis of Ppa fluorescence intensity in 4T1 cells after their incubation with glycopolymer-PTX-DOTA-Gd at different durations. (C) Cytotoxicity of glycopolymer-PTX-DOTA-Gd and free PTX against 4T1 cells (mean ± SD, $n = 5$). (D) Penetration of glycopolymer-PTX-DOTA-Gd into MTS of 4T1 cell using a CLSM after incubation for 2 h and 6 h. The images of the spheroids were captured at every 10 μm from the bottom to the middle of the spheroids. For each sample, the blue fluorescence for the nuclei stained with Hoechst33342, while the purple fluorescence for glycopolymer-PTX-DOTA-Gd labelled with Ppa. Scale bar: 50 μm. (E) The fluorescence signal distribution along the direction marked, and (F) 3D topological images for penetration of glycopolymer-PTX-DOTA-Gd into one MTS at a depth of 70 μm. (G) CLSM images of MTSs incubated with free PTX or glycopolymer-PTX-DOTA-Gd for 48 h. The green fluorescence for live cells stained with Calcein-AM, and the red fluorescence for dead cells stained with PI. Scale bar: 50 μm.

1.5 T MRI system. As shown in Fig. 2C, a brighter signal is acquired from the glycopolymer-PTX-DOTA-Gd group in comparison with the Gd-DTPA group at an equivalent $Gd^{3+}$ concentration. In Fig. 2D, a linear correlation between the relaxivity of glycopolymer-PTX-DOTA-Gd and the $Gd^{3+}$ concentration is obtained for prodrug-based nanoparticles and clinical agent Gd-DTPA with the $R^2$ for both lines close to 1.0. The relaxivity efficacy, $r_1$, of glycopolymer-PTX-DOTA-Gd was calculated to be 7.1 L/(mmol·s), 1.97 times of that of Gd-DTPA ($r_1 = 3.6$). The relaxivity efficacy of multi-amino and multi-

carboxylic compounds conjugated with small gadolinium molecules used for clinical diagnosis is mainly determined by their rotational correlation time ($\tau_R$). A decrease in $\tau_R$ by increasing the MW of the contrast agent results in an increase in the relaxivity efficacy. In our design, the small molecule Gd-DOTA is covalently attached onto the glycopolymer to dramatically increase the relaxivity efficacy with a great contrast ratio for MRI. Meanwhile, self-assembly and stability of glycopolymer-PTX-DOTA-Gd in an aqueous environment ensure a good linear correlation between this $Gd^{3+}$ compound and the $T_1$ relaxivity efficacy. The results indicate glycopolymer-PTX-DOTA-Gd is an effective contrast agent with a higher relaxivity efficacy than the clinical agent Gd-DTPA.

### 3.3. *In vitro cellular uptake and cytotoxicity*

Because of the presence of the covalently bonded fluorescence dye Ppa in glycopolymer-PTX-DOTA-Gd, CLSM was employed to observe the cellular uptake of this polymer conjugate through detecting the fluorescence of Ppa. Fig. 3A shows that the majority of glycopolymer-PTX-DOTA-Gd is distributed in the cytoplasm of 4T1 cells. After incubation, increasing fraction of the Ppa

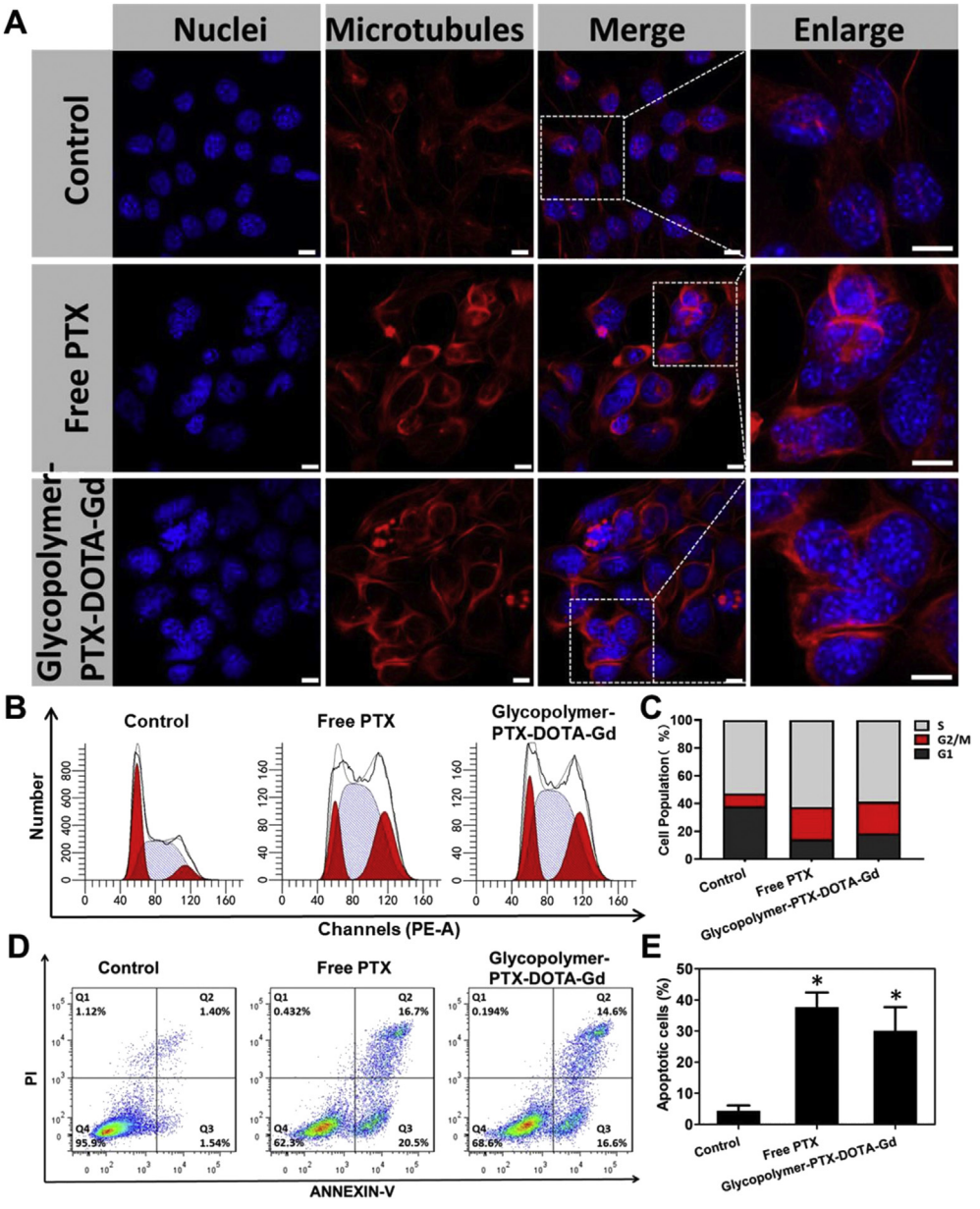


**Figure 4** (A) Microtubule aggregation of 4T1 cells treated by glycopolymer-PTX-DOTA-Gd prodrug-based nanoparticles and free PTX. Red fluorescence for microtubules stained with tubulin-tracker red, while blue fluorescence for nuclei stained with DAPI. Scale bar: 10 μm. (B) Cell cycle distribution and (C) semi-quantitative analysis of the 4T1 cells treated by nanoparticles and free PTX. (D) Apoptosis and semi-quantitative analysis (E) of 4T1 cells treated by nanoparticles and free PTX (*$P < 0.01$, compared to control, mean ± SD, $n = 3$). Cells treated with fresh medium are used as a control.

fluorescence from glycopolymer-PTX-DOTA-Gd overlapped with the lysosome fluorescence stained by Lyso-Tracker, indicating that prodrug-based nanoparticles may be taken up by cells through the endocytosis lysosomal pathway. A continuous increase in the Ppa fluorescence intensity is observed with extension of the incubation time, which is supported by flow cytometric analysis of 4T1 cells after uptake of glycopolymer-PTX-DOTA-Gd (Fig. 3B).

After cellular uptake of glycopolymer-PTX-DOTA-Gd, its cytotoxicity in 4T1 cells was tested by the CCK-8 analysis method. The glycopolymer conjugate was incubated with 4T1 cells for 48 h. Fig. 3C indicates that the cytotoxicity of both free PTX and glycopolymer-PTX-DOTA-Gd against 4T1 cells is concentration-dependent. As the concentration of both PTX and glycopolymer-PTX-DOTA-Gd increase, the viable cells decrease accordingly. However, glycopolymer-PTX-DOTA-Gd has a higher $IC_{50}$ of 1.99 μmol/L, the concentration of the therapeutic product at which 50% of cells are inhibited. The $IC_{50}$ of glycopolymer-PTX-DOTA-Gd is 1.7 times of that of free PTX (1.17 μmol/L), which may be explained by a different endocytosis and drug release process of the prodrug-based nanoparticles compared to the free diffusion of small molecule PTX.

The two-dimensional cytotoxicity assessment through 4T1 cell culture has revealed an equivalent antitumor effect of glycopolymer-PTX-DOTA-Gd as free PTX. The antitumor effect was further confirmed by applying the conjugate to 3D MTSs. Penetration of glycopolymer-PTX-DOTA-Gd through 4T1 MTSs was first evaluated. It can be seen from the topological 3D view images and CLSM images (Fig. 3D–F) that a great amount of glycopolymer-PTX-DOTA-Gd is observed to locate on the periphery of MTSs after treatment for 2 h. Significantly broader and stronger signals are observed after extending incubation up to 6 h, supporting deep penetration of glycopolymer-PTX-DOTA-Gd into 3D MTSs.

The antitumor activity of glycopolymer-PTX-DOTA-Gd against 3D MTSs was also demonstrated. Staining profiles of MTSs are summarized in Fig. 3G. The green fluorescence for live cells is stained with CAM, and the red fluorescence for dead cells is stained with PI. The growth profiles of MTSs are showed in Supporting Information Fig. S4. An abnormal morphology and a large area of collapsed death cells are observed from MTSs incubated with glycopolymer-PTX-DOTA-Gd and treated with free PTX. A significant increase in PI-positive (dead) areas is found in both MTSs treated with free PTX and glycopolymer-PTX-DOTA-Gd after incubation for 48 h. The abnormal morphology of the death cells might for the long incubation time and their necrosis. Thus, glycopolymer-PTX-DOTA-Gd

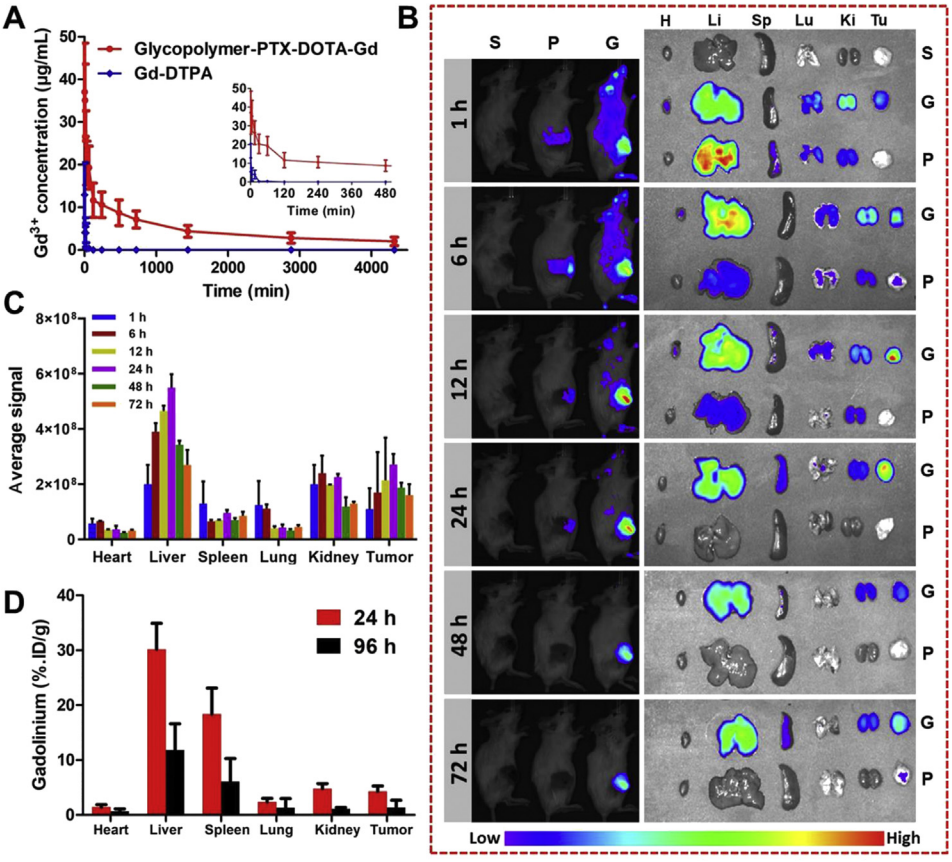


**Figure 5** (A) Temporal changes of $Gd^{3+}$ concentrations in the blood of BALB/c mice after injection of Gd-DTPA and glycopolymer-PTX-DOTA-Gd (mean ± SD, $n = 5$); (B) Fluorescence images of tumor-bearing mice, main organs and tumor tissues of mice after administration of the prodrug-based nanoparticles and free Ppa. S: saline, G: Glycopolymer-PTX-DOTA-Gd, P: Ppa, H: heart, Li: liver, Sp: spleen, Lu: lung, Ki: kidney, Tu: tumor. (C) Semi-quantitative fluorescence signal intensity for prodrug-based nanoparticles after administration into mice at 1, 6, 12, 24, 48 and 72 h post-injection (mean ± SD, $n = 3$). (D) Distribution of glycopolymer-PTX-DOTA-Gd at major organs and tumor (mean ± SD, $n = 5$).

demonstrates its ability in deep penetration into three dimensional solid tumors and equivalent antitumor effect compared to free PTX.

The main antitumor mechanism of PTX is reported to stabilize microtubules through depolymerization of them by selectively binding PTX to $\beta$-monomers[47]. The microtubules of 4T1 cells (Fig. 4A) were observed after tubulin staining. The normal microtubules labeled by Tubulin-Tracker Red are uniformly distributed as lattices inside 4T1 cell. Aggregation of microtubules and multi-nuclei are observed in one cell after treatment with prodrug-based nanoparticles and free PTX, revealing stabilization of microtubules in the treated groups during cell division. This suggests the same antitumor mechanism and effect of glycopolymer-PTX-DOTA-Gd compared to free PTX.

Cell proliferation cycle is an important parameter to reveal the proliferation state of cells. As shown in Fig. 4B and C, the proliferation state of 4T1 cells without treatment shows that its G1 phase (37.84%) is significantly higher than its G2/M phase (9.39%). However, the fraction of the G1 and G2/M phase is found to be 14.06% and 23.34% in 4T1 cells treated with free PTX, while the G1 and G2/M phase of 4T1 cells treated with glycopolymer-PTX-DOTA-Gd is 18.33% and 22.98%, respectively, indicating inhibition of cell proliferation cycles by free PTX and an equivalent inhibition effect by glycopolymer-PTX-DOTA-Gd.

The Annexin V-FITC double-staining method was further utilized for differentiation of non-apoptosis, early apoptosis, and late apoptosis of 4T1 cells induced by free PTX and

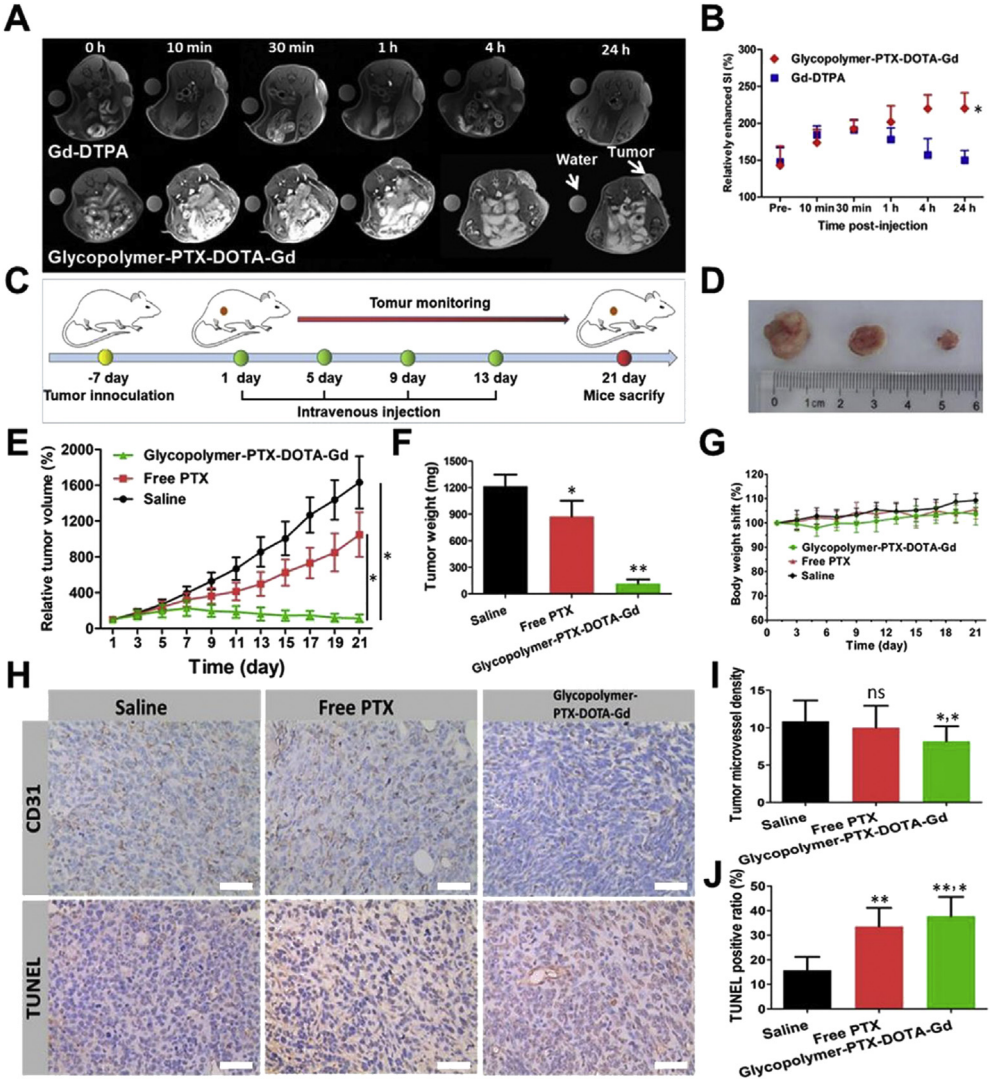


**Figure 6** (A) Imaging efficacy: representative MRI images and (B) the relative enhancement of the signal-to-noise ratio (ΔSNR) at the tumor site in BALB/c mice after administration of prodrug-based nanoparticles or Gd-DTPA (*$P$<0.05, mean ± SD, $n$ = 5); (C) glycopolymer-PTX-DOTA-Gd treatment strategy. (D) The representative tumor tissue photograph for each group after finish treatment. (E) Relative tumor volumes in different treatment groups (*$P$<0.01, compared to saline group and free PTX group, mean ± SD, $n$ = 7). (F) Tumor weights treated by free PTX and glycopolymer-PTX-DOTA-Gd (*$P$ < 0.01, **$P$ < 0.001, compared to saline, mean ± SD, $n$ = 7); (G) Body weight shift of mice in each group after treatment in 21 days (mean ± SD, $n$ = 5). (H) Immunohistochemical images for TUNEL and CD31 staining of tumor tissues (scale bar = 50 μm), and semi-quantitative data for (I) CD31 and (J) TUNEL (*$P$ < 0.05, **$P$ < 0.01, compared to saline; ns, nonsignificant, mean ± SD, $n$ = 3).

glycopolymer-PTX-DOTA-Gd. Both free PTX and glycopolymer-PTX-DOTA-Gd have successfully induced apoptosis of 4T1 cells: 37.2% cellular apoptosis (including early and late stage of apoptosis) for free PTX and 31.2% for glycopolymer-PTX-DOTA-Gd (Fig. 4D and E). Both cell viability and apoptosis results demonstrate the chemotherapeutic effectiveness of glycopolymer-PTX-DOTA-Gd against tumor cells.

### 3.4. *Pharmacokinetics and biodistribution of glycopolymer-PTX-DOTA-Gd*

The pharmacokinetic characteristics of glycopolymer-PTX-DOTA-Gd were analyzed by detecting of the $Gd^{3+}$ concentration in the blood of BALB/c female mice. As shown in Fig. 5A, Gd-DTPA, an MRI agent used in clinical practices, has a rapid blood clearance rate and no $Gd^{3+}$ in the blood is detectable after injection of Gd-DTPA into mice for 1 h. On the contrary, a concentration of $Gd^{3+}$ up to 10 μg/mL is found at 4 h post-injection of glycopolymer-PTX-DOTA-Gd into mice and 7 μg/mL at 12 h post-injection, indicating a significantly prolonged blood circulation time of glycopolymer-PTX-DOTA-Gd. The data for the $Gd^{3+}$ concentration with time were used to estimate the pharmacokinetic parameters *via* a two-compartment model and the parameters are summarized in Supporting Information Table S3. A very short half-time ($t_{1/2\beta}$ = 14.2 min) is found for Gd-DTPA in blood, but a relatively longer half-time ($t_{1/2\beta}$ = 1255.4 min) for glycopolymer-PTX-DOTA-Gd. Glycopolymer-PTX-DOTA-Gd also has a slower systematic clearance rate and a higher circulation time in comparison with Gd-DTPA.

*In vivo* biodistribution of glycopolymer-PTX-DOTA-Gd was revealed by detecting the Ppa fluorescence in 4T1 xenograft mice after administration of the drug. Firstly, the fluorescence imaging of tumor-bearing mice showed the distribution characteristics at tumor site (Supporting Information Fig. S5). In the free Ppa-treated group, only low Ppa signals were detected. The highest signal appeared at 12 h post-injection. While in glycopolymer-PTX-DOTA-Gd-treated group, much higher Ppa signals in all time points, by contrast, were measured. The fluorescence signal continuously increases to the highest at 24 h post-injection and then decreases. Secondly, a further analysis for the organs and tumor tissues reveal more biodistribution information. A distinctive distribution of Ppa-conjugated glycopolymer-PTX-DOTA-Gd is found in liver and tumor of mice in comparison with free Ppa (Fig. 5B). In the free Ppa-treated group, at 1 h post-injection, strong fluorescence signals are observed in liver, while no signal is detectable at the tumor site, suggesting remarkable accumulation of free Ppa in liver. A continuous decline of the fluorescence signals within all organs is observed as the time of post-injection extends and almost no fluorescence signals are seen at 12 h post-injection. In the prodrug-based nanoparticles-treated group, a very low level of fluorescence signal intensity is observed in heart, lung and spleen, which is equivalent to that in these organs from free Ppa-treated mice. While in liver and tumor, the fluorescence signal initially increases to the highest at 24 h post-injection. The observations are also in agreement with the semi-quantitative analysis results shown in Fig. 5C for glycopolymer-PTX-DOTA-Gd. The semi-quantitative analysis results in Supporting Information Fig. S6 support the fluorescence signal changes that showed, too. The signal intensity in liver and tumor in the prodrug-treated group is significantly stronger than that in the free Ppa-treated group. The *in-vivo* biodistribution from fluorescence imaging of major organs and tumor suggests a higher circulation time of Ppa-conjugated glycopolymer-PTX-DOTA-Gd, and a higher level of tumor targeting owing to the EPR effect.

*In vivo* biodistribution of glycopolymer-PTX-DOTA-Gd was also revealed at 24 h and 96 h post-injection in major organs and tumor nodes by measuring the $Gd^{3+}$ concentration by ICP-MS. A trace amount of $Gd^{3+}$ is detected at 24 h post-injection in organs and tumor from the Gd-DTPA-treated mice: 0.1% ID/g $Gd^{3+}$ (0.2% of total injected $Gd^{3+}$ in the sample) in liver; 0.1% ID/g in tumor and less than 0.1% ID/g for other organs (Supporting Information Fig. S7). The sacrifice at 96 h for Gd-DTPA-treated mice was thus canceled for the extreme low concentration of $Gd^{3+}$ was detected in 24 h. This is in agreement with the result from fluorescence imaging. However, after 24 h of administration of glycopolymer-PTX-DOTA-Gd, a significant amount of $Gd^{3+}$ was observed in liver (30.9% ID/g) and spleen (18.4% ID/g), and only about 4.8% ID/g $Gd^{3+}$ occurred in kidney. Meanwhile, there was around 4.3% ID/g $Gd^{3+}$ was found in tumor tissue. At 96 h post-injection, the $Gd^{3+}$ concentration in liver and spleen deceases significantly: 11.9% in liver, and 6.1% in spleen; while a very small amount of $Gd^{3+}$ is found in tumor and other major organs (Fig. 5D). The toxicity of $Gd^{3+}$-based contrast agents is highly associated with nephrogenic systemic fibrosis (NSF), which occurs mostly on renal dysfunctional patients. Free $Gd^{3+}$ is highly toxic and the toxicity mechanism is believed to be associated with a long tissue exposure time, voltage-gated calcium channels blockage, tissue fibrosis associated with cytokines and inorganic Gd-phosphate precipitates formation[48]. While the use of macrocyclic $Gd^{3+}$ (DOTA-Gd) significantly reduced $Gd^{3+}$ retention post-injection at 96 h in mice that have normal renal function, preventing the occurrence of NSF caused by glycopolymer-PTX-DOTA-Gd. Although the temporal distribution of $Gd^{3+}$ is similar to the Ppa distribution (fluorescence imaging) in major organs and tumor, $Gd^{3+}$ has a much rapid clearance rate after dissociation from glycopolymer-PTX-DOTA-Gd, while the Ppa-bonded glycopolymer and their degraded products are gradually cleared from the body. The $Gd^{3+}$/Ppa distribution indicates better accumulation of the glycopolymer conjugate than Gd-DTPA and negligible genotoxic potential of glycopolymer-PTX-DOTA-Gd through rapid metabolism after its MRI function.

### 3.5. *In vivo theranostic evaluation*

Female BALB/c mice with 4T1 tumor nodes were employed to evaluate the MRI efficacy of glycopolymer-PTX-DOTA-Gd prodrug-based nanoparticles and a clinical agent Gd-DTPA. The imaging contrast intensity of tumor against the tissue background in Fig. 6A becomes much brighter after extending the time post-injection of nanoparticles into mice, while the contrast intensity in the Gd-DTPA-treated group is enhanced only in the first 30 min post-injection and then fades out slowly down to the same intensity level at 4 h post-injection as that at pre-injection. The relative enhanced intensity signal (SI) in the tumors was further calculated as the ratio of the contrast intensity at the tumor site to that of water at the same detection time and the calculated values for nanoparticles and Gd-DTPA are shown in Fig. 6B. The relative enhanced SI at the tumor site keeps increasing even after 24 h of injection of nanoparticles although the incremental change in the relatively enhanced SI is much smaller between 4 and 24 h in comparison with the changes within 4 h post-injection. However, in the Gd-DTPA-treated group, the relative enhanced SI rises to a peak in the first 30 min post-injection and then rapidly declines after 30 min. From 1 h post-injection onwards, the relative

enhanced SI for nanoparticles is higher than that for Gd-DTPA. Therefore, the MRI function of nanoparticles through complexion of Gd-DTPA with the glycopolymer is significantly enhanced up to 24 h post-injection, and this allows monitoring of the tumor site for a much longer time in comparison with 30 min for Gd-DTPA.

The anti-tumor therapeutic efficacy was assessed in 4T1 breast tumor xenograft mice through characterizing the tumor with time after administration of saline, free PTX or glycopolymer-PTX-DOTA-Gd for 4 times (Fig. 6C). As shown in Fig. 6D and E, after injection of saline, PTX and glycopolymer-PTX-DOTA-Gd into mice, tumor grows rapidly in the saline-injected group and the volume reaches 1631% on day 21 post-injection, while tumor has a similar tumor growth rate in the PTX-injected group as the saline-injected group in the first 7 days, and then the growth rate starts to slow down after 7 days, and the volume (1049%) is smaller than that in the saline group on Day 21. On the contrast, the change for glycopolymer-PTX-DOTA-Gd group showed an opposite temporal profile. After the first injection of glycopolymer-PTX-DOTA-Gd, the tumor growth is observed to be slower than other two groups. Because it takes time for nanoparticles concentration at the tumor site, penetration into tumors and drug release inside the tumors, the tumor volume does not start to decrease instantly, but on Day 7 repeat injection of glycopolymer-PTX-DOTA-Gd results in a continuous decrease in the tumor volume and this decreasing pattern keeps until Day 21. The solid tumor is significantly inhibited by injection of glycopolymer-PTX-DOTA-Gd with a very small volume on Day 21 comparing with the saline and PTX groups, and some tumors have been completely eradiated through treatment by glycopolymer-PTX-DOTA-Gd.

To confirm the tumor volume changes after 21-day treatment by saline, free PTX and glycopolymer-PTX-DOTA-Gd, tumors from all sacrificed mice on day 21 were resected and weighed. The tumor weight of mice treated by glycopolymer-PTX-DOTA-Gd (114.0 $\pm$ 49.1 mg) is the lightest, and the tumor is dramatically shrunk in comparison with that in the free PTX group (873.8 $\pm$ 178.1 mg) and the saline group (1214.1 $\pm$ 133.1 mg, Fig. 6F). The tumor growth inhibition (TGI) by glycopolymer-PTX-DOTA-Gd reaches up to 90.6%, on the contrast, the TGI by free PTX is only at 28.0% (Supporting Information Fig. S8). Meanwhile, the weight of each mouse in all groups was monitored and all mice have a very similar weight up to 21 days after injection of saline, free PTX and glycopolymer-PTX-DOTA-Gd (Fig. 6G). Therefore, glycopolymer-PTX-DOTA-Gd has been demonstrated with a better antitumor efficacy due to its higher blood circulation time, better accumulation at tumor sites and rapid release of the therapeutic agent triggered by the tumor specific microenvironment, as well as excellent biosafety due to its great stability in the blood circulation and rapid clearance from the body after its therapeutic effect. H&E staining was employed to assess the histological changes of major organs in each mouse after injection of glycopolymer-PTX-DOTA-Gd, free PTX and saline. As shown in Supporting Information Fig. S9, there is no observable toxicity to the selected organs in three experiment groups, except livers in both saline and free PTX groups with severe infiltration of inflammatory cells.

The antitumor mechanisms of glycopolymer-PTX-DOTA-Gd at the cellular level were revealed through an immunohistochemical method to assess the histopathologic characteristics of tumor tissues after treatment. Specifically, CD31 staining was used to evaluate angiogenesis, and TUNEL for programmed cell death (Fig. 6H). Angiogenesis is a vital process in proliferation and metastasis of most solid tumors, and anti-angiogenesis may contribute to tumor suppression. In Fig. 6I, there is a remarkable statistical significance ($P < 0.05$) for the micro vessel density (MVD) in the tumor tissue represented by CD31 positive cell counts between the glycopolymer-PTX-DOTA-Gd group and the saline group, while no statistical significance ($P > 0.05$) is found when the PTX group is compared with the saline group, indicating glycopolymer-PTX-DOTA-Gd induces better anti-angiogenesis in tumor tissues than free PTX.

Fig. 6J reveals that the ratio of apoptotic cells to viable cells is 37.7% after TUNEL staining of the tumor tissue treated by glycopolymer-PTX-DOTA-Gd, which is higher than that from the PTX-treated group (33.6%) and saline-treated group (15.7%). These immunochemical staining results demonstrate that glycopolymer-PTX-DOTA-Gd has the highest efficacy in tumor suppression against 4T1 tumors through preventing tumor angiogenesis and progression, and inducing apoptosis or necrosis of tumor cells.

## 4. Conclusions

We have successfully constructed a multifunctional drug delivery system based on a glycopolymer carrier. Gd-DOTA, PTX and Ppa are integrated into the glycopolymer to self-assemble into nanoparticles (glycopolymer-PTX-DOTA-Gd). Glycopolymer-PTX-DOTA-Gd has been demonstrated to have better pharmacokinetics with a longer blood half-time, greater tumor accumulation, brighter MRI contrast intensity for up to 24 h in comparison with Gd-DTPA. Glycopolymer-PTX-DOTA-Gd also has a higher therapeutic efficacy with a TGI of more than 90% than free PTX by inhibiting angiogenesis, progression and proliferation of 4T1 xenograft because PTX is rapidly released from the glycopolymer carrier in the tumor microenvironment. Therefore, this multifunctional drug delivery system derived from the glycopolymer prodrug may have a great potential in theranostics for cancer treatment.

## Acknowledgments

This research was financially supported by the National Natural Science Foundation of China (Nos. 51873120, 51673127, and 81621003), Department of Science and Technology of Sichuan Province (Nos. 2018JY0574, 2017SZ0006, 18GJHZ0139, and 2018HH0006, China), and 1·3·5 Research Funds in West China Hospital of Sichuan University (ZYGD18028, China). We are grateful to Sisi Wu, Xuemei Chen, Yanjing Zhang, Yan Wang, Fengfeng Chen, Yinchan Wang, Jie Zhang, Bo Su and Yi Zhang (Core Facility of West China Hospital, Sichuan University, China) for their help in *in vitro* and *in vivo* studies.

## Author contributions

Kui Luo and Yanhui Liu designed the project. Hao Cai, Yufan Xiang, Yujun Zeng, Zhiqian Li, Qiang Luo, and Kui Luo performed the experiments. Kui Luo provided experimental drugs and quality control. Hao Cai, Yufan Xiang, and Yanhui Liu acquired, analyzed and interpreted the data. Hao Cai, Yufan Xiang, Xiuli Zheng, and drafted the manuscript and Hu Zhang, Qiyong Gong, Zhongwei Gu, Yanhui Liu, Hu Zhang and Kui Luo

critically revised the manuscript. All of the authors have read and approved the final manuscript.

## Conflicts of interest

The authors have no conflicts of interest to declare.

## Appendix A. Supporting information

Supporting data to this article can be found online at https://doi.org/10.1016/j.apsb.2020.07.023.

## References


1. Zhou Q, Shao S, Wang J, Xu C, Xiang J, Piao Y, et al. Enzyme-activatable polymer-drug conjugate augments tumour penetration and treatment efficacy. *Nat Nanotechnol* 2019;**14**:799−809.
2. Battogtokh G, Choi YS, Kang DS, Park SJ, Shim MS, Huh KM, et al. Mitochondria-targeting drug conjugates for cytotoxic, anti-oxidizing and sensing purposes: current strategies and future perspectives. *Acta Pharm Sin B* 2018;**8**:862−80.
3. Li N, Zhao L, Qi L, Li Z, Luan Y. Polymer assembly: promising carriers as co-delivery systems for cancer therapy. *Prog Polym Sci* 2016;**58**:1−26.
4. Seidi F, Jenjob R, Crespy D. Designing smart polymer conjugates for controlled release of payloads. *Chem Rev* 2018;**118**:3965−4036.
5. Li C, Wang J, Wang Y, Gao H, Wei G, Huang Y, et al. Recent progress in drug delivery. *Acta Pharm Sin B* 2019;**9**:1145−62.
6. Wang L, Quan P, Chen SH, Bu W, Li YF, Wu X, et al. Stability of ligands on nanoparticles regulating the integrity of biological membranes at the nano-lipid interface. *ACS Nano* 2019;**13**:8680−93.
7. Larson N, Ghandehari H. Polymeric conjugates for drug delivery. *Chem Mater* 2012;**24**:840−53.
8. Liu E, Zhang M, Cui H, Gong J, Huang Y, Wang J, et al. Tat-functionalized Ag-$Fe_3O_4$ nano-composites as tissue-penetrating vehicles for tumor magnetic targeting and drug delivery. *Acta Pharm Sin B* 2018;**8**:956−68.
9. Mi P, Cabral H, Kataoka K. Ligand-installed nanocarriers toward precision therapy. *Adv Mater* 2020;**32**:e1902604.
10. Zheng X, Pan D, Chen M, Dai X, Cai H, Zhang H, et al. Tunable hydrophile-lipophile balance for manipulating structural stability and tumor retention of amphiphilic nanoparticles. *Adv Mater* 2019;**31**:1901586.
11. Miao T, Wang J, Zeng Y, Liu G, Chen X. Polysaccharide-based controlled release systems for therapeutics delivery and tissue engineering: from bench to bedside. *Adv Sci* 2018;**5**:1700513.
12. Šírová M, Strohalm J, Chytil P, Lidický O, Tomala J, Říhová B, et al. The structure of polymer carriers controls the efficacy of the experimental combination treatment of tumors with HPMA copolymer conjugates carrying doxorubicin and docetaxel. *J Control Release* 2017;**246**:1−11.
13. Zhang P, Zhang L, Qin Z, Hua S, Guo Z, Chu C, et al. Genetically engineered liposome-like nanovesicles as active targeted transport platform. *Adv Mater* 2018;**30**:1705350.
14. Rihova B, Kovar L, Kovar M, Hovorka O. Cytotoxicity and immunostimulation: double attack on cancer cells with polymeric therapeutics. *Trends Biotechnol* 2009;**27**:11−7.
15. Gaspar R, Duncan R. Polymeric carriers: preclinical safety and the regulatory implications for design and development of polymer therapeutics. *Adv Drug Deliv Rev* 2009;**61**:1220−31.
16. Kim D, Le QV, Kim YB, Oh YK. Safety and photochemotherapeutic application of poly($\gamma$-glutamic acid)-based biopolymeric nanoparticle. *Acta Pharm Sin B* 2019;**9**:565−74.
17. Du C, Ding Y, Qian J, Zhang R, Dong CM. Achieving traceless ablation of solid tumors without recurrence by mild photothermal-chemotherapy of triple stimuli-responsive polymer−drug conjugate nanoparticles. *J Mater Chem B* 2019;**7**:415−32.
18. Jin Q, Deng Y, Chen X, Ji J. Rational design of cancer nanomedicine for simultaneous stealth surface and enhanced cellular uptake. *ACS Nano* 2019;**13**:954−77.
19. Chen B, Dai W, He B, Zhang H, Wang X, Wang Y, et al. Current multistage drug delivery systems based on the tumor microenvironment. *Theranostics* 2017;**7**:538−58.
20. Liu R, Hu C, Yang Y, Zhang J, Gao H. Theranostic nanoparticles with tumor-specific enzyme-triggered size reduction and drug release to perform photothermal therapy for breast cancer treatment. *Acta Pharm Sin B* 2019;**9**:410−20.
21. Du C, Ding Y, Qian J, Zhang R, Dong CM. Dual drug-paired polyprodrug nanotheranostics reverse multidrug resistant cancers *via* mild photothermal-cocktail chemotherapy. *J Mater Chem B* 2019;**7**:5306−19.
22. Cai H, Dai X, Wang X, Tan P, Gu L, Luo Q, et al. A nanostrategy for efficient imaging-guided antitumor therapy through a stimuli-responsive branched polymeric prodrug. *Adv Sci* 2020;**7**:1903243.
23. Suriano F, Pratt R, Tan JP, Wiradharma N, Nelson A, Yang YY, et al. Synthesis of a family of amphiphilic glycopolymers *via* controlled ring-opening polymerization of functionalized cyclic carbonates and their application in drug delivery. *Biomaterials* 2010;**31**:2637−45.
24. Pearson S, Vitucci D, Khine YY, Dag A, Lu H, Save M, et al. Light-responsive azobenzene-based glycopolymer micelles for targeted drug delivery to melanoma cells. *Eur Polym J* 2015;**69**:616−27.
25. Miura Y, Hoshino Y, Seto H. Glycopolymer nanobiotechnology. *Chem Rev* 2016;**116**:1673−92.
26. Lau UY, Pelegri-O'Day EM, Maynard HD. Synthesis and biological evaluation of a degradable trehalose glycopolymer prepared by RAFT polymerization. *Macromol Rapid Commun* 2018;**39**:1700652.
27. Chen S, Sun B, Miao H, Wang G, Sun P, Li J, et al. NIR-II dye-based multifunctional telechelic glycopolymers for NIR-IIa fluorescence imaging-guided stimuli-responsive chemo-photothermal combination therapy. *ACS Mater Sci* 2020;**2**:174−83.
28. Mohammadifar E, Nemati Kharat A, Adeli M. Polyamidoamine and polyglycerol; their linear, dendritic and linear−dendritic architectures as anticancer drug delivery systems. *J Mater Chem B* 2015;**3**:3896−921.
29. Liu X, Lin W, Astruc D, Gu H. Syntheses and applications of dendronized polymers. *Prog Polym Sci* 2019;**96**:43−105.
30. Cook AB, Perrier S. Branched and dendritic polymer architectures: functional nanomaterials for therapeutic delivery. *Adv Funct Mater* 2019;**30**:1901001.
31. Van Bruggen C, Hexum JK, Tan Z, Dalal RJ, Reineke TM. Nonviral gene delivery with cationic glycopolymers. *Accounts Chem Res* 2019;**52**:1347−58.
32. Narain R, Armes SP. Synthesis of low polydispersity, controlled-structure sugar methacrylate polymers under mild conditions without protecting group chemistry. *Chem Commun* 2002;**23**:2776−7.
33. Zhang R, Yang J, Sima M, Zhou Y, Kopecek J. Sequential combination therapy of ovarian cancer with degradable *N*-(2-hydroxypropyl) methacrylamide copolymer paclitaxel and gemcitabine conjugates. *Proc Natl Acad Sci U S A* 2014;**111**:12181−6.
34. Sun L, Li X, Wei X, Luo Q, Guan P, Wu M, et al. Stimuli-responsive biodegradable hyperbranched polymer-gadolinium conjugates as efficient and biocompatible nanoscale magnetic resonance imaging contrast agents. *ACS Appl Mater Interfaces* 2016;**8**:10499−512.
35. Tang M, Zhou M, Huang Y, Zhong J, Zhou Z, Luo K. Dual-sensitive and biodegradable core-crosslinked HPMA copolymer−doxorubicin conjugate-based nanoparticles for cancer therapy. *Polym Chem-uk* 2017;**8**:2370−80.
36. Wei X, Luo Q, Sun L, Li X, Zhu H, Guan P, et al. Enzyme- and pH-sensitive branched polymer-doxorubicin conjugate-based nanoscale drug delivery system for cancer therapy. *Appl Mater Interfaces* 2016;**8**:11765−78.
37. Pan DY, Zheng XL, Zhang QF, Li ZQ, Duan ZY, Zheng W, et al. Dendronized-polymer disturbing cells' stress protection by targeting metabolism leads to tumor vulnerability. *Adv Mater* 2020;**32**:1907490.

38. Cai H, Wang XJ, Zhang H, Sun L, Pan DY, Gong QY, et al. Enzyme-sensitive biodegradable and multifunctional polymeric conjugate as theranostic nanomedicine. *Appl Mater Today* 2018;**11**:207−18.
39. Ryu JH, Na JH, Ko HK, You DG, Park S, Jun E, et al. Non-invasive optical imaging of cathepsin B with activatable fluorogenic nanoprobes in various metastatic models. *Biomaterials* 2014;**35**: 2302−11.
40. Parker BS, Ciocca DR, Bidwell BN, Gago FE, Fanelli MA, George J, et al. Primary tumour expression of the cysteine cathepsin inhibitor stefin A inhibits distant metastasis in breast cancer. *J Pathol* 2008;**214**: 337−46.
41. Zhang Y, Huo M, Zhou J, Xie S. PKSolver: an add-in program for pharmacokinetic and pharmacodynamic data analysis in Microsoft Excel. *Comput Methods Progr Biomed* 2010;**99**:306−14.
42. Guo C, Sun L, Cai H, Duan Z, Zhang S, Gong Q, et al. Gadolinium-labeled biodegradable dendron−hyaluronic acid hybrid and its subsequent application as a safe and efficient magnetic resonance imaging contrast agent. *ACS Appl Mater Interfaces* 2017;**9**:23508−19.
43. Li N, Li N, Yi Q, Luo K, Guo C, Pan D, et al. Amphiphilic peptide dendritic copolymer-doxorubicin nanoscale conjugate self-assembled to enzyme-responsive anti-cancer agent. *Biomaterials* 2014;**35**: 9529−45.
44. Hickey JW, Santos JL, Williford JM, Mao HQ. Control of polymeric nanoparticle size to improve therapeutic delivery. *J Control Release* 2015;**219**:536−47.
45. Chen K, Liao S, Guo S, Zheng X, Wang B, Duan Z, et al. Multi-stimuli-responsive PEGylated polymeric bioconjugate-based nano-aggregate for cancer therapy. *Chem Eng J* 2020;**391**:123543.
46. Chen K, Cai H, Zhang H, Zhu H, Gu Z, Gong Q, et al. Stimuli-responsive polymer-doxorubicin conjugate: antitumor mechanism and potential as nano-prodrug. *Acta Biomater* 2019;**84**:339−55.
47. Xiao H, Verdier-Pinard P, Fernandez-Fuentes N, Burd B, Angeletti R, Fiser A, et al. Insights into the mechanism of microtubule stabilization by Taxol. *Proc Natl Acad Sci U S A* 2006;**103**:10166−73.
48. Todd DJ, Kay J. Gadolinium-induced fibrosis. *Annu Rev Med* 2016;**67**: 273−91.